Annals of Glaciology 27 1998

Near-coastal iceberg distributions in East Antarctica, 50–145° E

N.W. Young,[1] D. Turner,[1] G. Hyland,[1] R. N. Williams[2]
[1]*Antarctic CRC and Australian Antarctic Division, Box 252-80, Hobart, Tasmania 7001, Australia*
[2]*Department of Computing, University of Tasmania, P.O. Box 1214, Launceston, Tasmania 7250, Australia*

ABSTRACT. A survey of icebergs using satellite radar images has been made in the seasonal sea-ice zone of East Antarctica in the sector between longitudes 50° and 145° E. These data provide information on the spatial distribution and size statistics of icebergs near the coast in areas not often visited by shipboard observers, and close to their sources at ice shelves and glacier tongues. The icebergs are detected and their dimensions extracted by analysis of the texture properties present in satellite images acquired with ERS-1 synthetic aperture radar during the austral winter. The minimum size of iceberg reliably detected and measured is 0.06 km^2.

A significant variation, by up to a factor of two, is found in the area of icebergs close to different sections of the coast, which suggests a characteristic size for different sources. The average value of the length-to-width ratio for icebergs in the whole population shows some variability with size. The probability of finding icebergs is greatest close to the coast, decreasing in general with distance from the coast, such that few icebergs were detected more than 160 km from the coast. In one sector about 85° E, icebergs are found to at least 550 km from the coast, which is consistent with the transport of icebergs northwards in this region by a branch of the westward-heading near-coastal current (East Wind Drift) which connects with the southern margins of the eastward-heading Antarctic Circumpolar Current.

1. INTRODUCTION

Icebergs represent the largest single component of the mass flux discharged from the Antarctic ice sheet. They calve mostly from the margins of ice shelves and glacier tongues, which occupy approximately 44% and 13% of the coastline, respectively. Ice cliffs in contact with the ocean comprise about another 38% of the coastline and contribute a smaller fraction of the mass flux discharged as icebergs. Most of the remainder of the mass discharge occurs through melting from the base of ice shelves and from beneath glaciers and ice streams. Tabular bergs up to gigantic proportions usually calve from ice shelves. Glacier tongues generally produce more numerous and smaller tabular bergs, although large glacier tongues, such as Thwaites Glacier in West Antarctica, can produce gigantic icebergs (Ferrigno and others, 1993). The break-up of ice shelves can also generate many small icebergs (Rott and others, 1996). Icebergs calved from ice cliffs tend to be small.

Icebergs from the various sources are intermingled and carried around Antarctica under the influence of ocean currents, eddies and surface winds. The larger icebergs (of a few kilometres and more), which drift mainly with the currents, act as tracers of these currents. Measurement of their drift can give a representative view of the current patterns (e.g. Tchernia and Jeannin, 1984). The possible impact at the margins of the Antarctic ice cover of a change in sea state after removal of the sea-ice cover or a rise in ocean temperature can be deduced from a study of the dissolution rate of icebergs through fracturing and melting (e.g. Hamley and Budd, 1986).

The prime source of information about the size and spatial distribution of icebergs in the oceans about Antarctica has to date been the data gathered by ship-borne observers. These observations have been collected over many years. Each set represents a snapshot of conditions along the routes taken by the various ships at the time of passage. Collation of these data provides a statistical picture of the sizes of icebergs and their dispersal by the ocean currents. From this it is estimated that there are 200 000–300 000 icebergs in the Southern Ocean south of the Antarctic Convergence (Orheim, 1988). Their sizes range from a linear dimension of about 50 m to tens of kilometres and occasionally in excess of 100 km. Many of the icebergs observed at sea are the product of fracturing and erosion of larger icebergs. Little is known about the actual numbers and sizes of icebergs produced when they first calve from their source at the edge of the ice sheet. In addition, it has not been possible to obtain a synoptic view of their distribution over a large sector of the ocean.

Analysis of images acquired by remote-sensing satellite systems provides an alternative source of data on the distribution and size of icebergs. Large Antarctic icebergs have been observed in images from a variety of systems starting with the first weather satellites (e.g. Swithinbank and others, 1977), as well as current systems operating in visible,

near-infrared, infrared and passive microwave (e.g. Phillips and Laxon, 1995). High-resolution systems such as Landsat and Système probatoire pour l'observation de la terre (SPOT) can provide information on the distribution of icebergs down to a size limit of the order of 50–100 m (e.g. Hult and Ostrander, 1974; Mead, 1992). But the utility of these visible wavelength systems is limited by the high frequency of cloud cover over the seasonal sea-ice zone and the lack of solar illumination in the winter months. Satellite-borne active microwave systems in the form of high-resolution synthetic aperture radar (SAR) and low-resolution scatterometer systems, can be used to observe the ocean surface independent of weather and incident lighting conditions. They provide the possibility of undertaking ocean-wide surveys over a short time interval. Regular acquisition of images over an extended period of time offers the opportunity to observe directly the calving of icebergs, their drift with the ocean currents and progressive decay by melting and fracturing (Young and Hyland, 1997), as well as episodic events such as the break-up of ice shelves (Rott and others, 1996).

In this work we use an image analysis technique to detect icebergs and define their outlines in SAR images of the seasonal sea-ice zone about East Antarctica in order to derive their spatial distribution and sizes. The technique uses the texture properties of the images to define closed segments of relatively homogeneous character and a threshold test on the intensity values to distinguish icebergs from false identifications. Attributes such as the centroid, area, mean intensity, etc., are extracted from the image segment for each positively identified iceberg. We have applied this technique to 54 European remote-sensing satellite (ERS-1) SAR images for which an initial assessment showed that icebergs were present in the image. These were selected from a much larger number of images distributed along the Antarctic coastline in a number of discrete regions between longitudes 50° and 145° E. The other images typically contained no detectable icebergs or no more than five small icebergs. We then use these iceberg identifications to investigate the dispersion of icebergs around the coast, and the character of the size distributions for each source region.

2. CHARACTER OF ICEBERGS IN SAR IMAGES

Willis and others (1996) described the mechanisms which contribute to the microwave backscatter character of icebergs relevant to their detection in radar images, such as those acquired by the ERS-1 SAR instrument. In the Antarctic during the cold winter months, icebergs generally appear as bright objects against a darker background of sea ice or ocean. In radar images the value of the backscatter coefficient of an iceberg is related partly to the roughness of its upper surface and partly to volume scattering from within the near-surface layers. Volume scattering is more effective when the bubble and crystal size of the ice is large and a significant fraction of the wavelength of the radar signal. The backscatter is strongest when the surface is composed of coarse-grain snow which is frozen and dry. A background consisting of a mixture of sea-ice types and open water has a lower average backscatter. In one of the study regions near longitude 140° E, Lytle and others (1997) using images from the C-band ERS-1 SAR found that large floes of first-year ice had an average backscatter coefficient of −12.4 dB, while thin ice types and open water in relatively calm conditions had a backscatter of less than −16.5 dB. Areas of sea ice which included up to 30% concentration of multi-year floes had backscatter values of −9.8 dB. Backscatter values up to −7 dB could be reached with a higher concentration of multi-year floes, but this is rare in the East Antarctic sea-ice zone.

A manual interpretation was made of sub-regions in three SAR images acquired during the winter month of August 1993 to identify icebergs on the basis of the texture of the image, and brightness. It showed that average values of the backscatter coefficient for positively identified icebergs are typically in the range −6 to −4 dB or higher. The icebergs in the images are mostly surrounded by first-year sea ice and partly by areas of open water or thin ice. 99% of the image pixels in this background have backscatter values of less than −10.5 dB, so the contrast in backscatter value between many of the icebergs and the darker background is typically about 5 dB and up to 10 dB.

This observation of icebergs being represented as bright objects against a darker background, however, cannot be applied as a universal criterion for the detection of icebergs in a SAR image. Icebergs can exhibit a much lower backscatter coefficient, and the background sea ice and ocean surface can also appear bright. The wind-roughened surface of open water exhibits a strong backscatter character which is dependent on the relative orientation of the wind direction and look direction of the radar. The average backscatter from sea ice increases as it is broken into smaller floes (Lytle and others, 1997). An increase of snow-moisture content on the surface of icebergs associated with melting of the surface snow induces a marked decrease in the backscatter. Young and Hyland (1997) found depression of the backscatter by 10 dB or more in association with strong melt events in some summer seasons in a study of very large icebergs using the ERS wind scatterometer which operates at the same wavelength as the SAR instrument. Icebergs that have lost their snow cover, either by ablation or by roll-over, appear dark. This will frequently occur as they fragment and melt with increasing age. Backscatter from individual icebergs greater than 1 km^2 in area that were uniquely identified more than once in a large sample of the SAR images was observed to vary by ± 1 dB and sometimes more over periods of days to weeks in the winter. The backscatter of these icebergs occurring within a single region changed in a consistent sense, probably reflecting a widespread effect of changing weather conditions. Thus, even a small reduction in the backscatter from an iceberg or change in the physical character of the background could remove the contrast between an iceberg and its neighbourhood, or even reverse the contrast so the iceberg appears as a dark object against a brighter background.

Because of the range of backscatter values exhibited by icebergs and the variety of conditions relating to their contrast against the background, a simple threshold technique to detect icebergs in SAR images is likely to have limited application. For this reason, the technique for detection of icebergs described by Williams (personal communication, 1997) was developed to take advantage of the texture properties exhibited by the SAR images and the different ice and water components present in them. Most of the SAR images currently available at the Cooperative Research Centre for Antarctic and Southern Ocean Environment for this project were acquired during winter months, and only a few

https://doi.org/10.3189/1998AoG27-1-68-74 Published online by Cambridge University Press

images from the summer months. To simplify analysis and interpretation of the results, images only from the winter months are used in this work. They were acquired during the periods: for longitudes 50–110° E, 6–23 August 1993 and 4–17 August 1994; for longitudes 130–145° E, 1 August–29 September 1995.

3. IMAGE ANALYSIS TECHNIQUE

Williams and others (personal communication, 1997) developed a technique to detect icebergs in SAR images and define their boundaries using an adaptation of a technique described by Sephton and others (1994) for segmenting sea-ice floes in SAR images. It uses the texture information in an image to distinguish areas of inhomogeneity separating regions of relatively homogeneous character in the images. Edges are constructed around the homogeneous regions, and further tests applied in order to differentiate which of these regions represent icebergs. The system has been implemented as a semi-automated procedure where an operator can interact with the system to select a sub-region of an image for analysis, adjust a threshold criteria value and verify and edit the analysis. The main stages in this procedure are summarised below.

The images are first pre-processed by applying an 8 pixel by 8 pixel block averaging filter which smooths the image by reducing the speckle "noise" inherent in SAR images. The smoothed images have a pixel size of 100 m by 100 m. A simple statistically based edge detector, the "sigma-on-mu" filter (Sephton and others, 1994), is then applied to the smoothed image to define areas of inhomogeneity. This filter is sensitive to the presence of an edge irrespective of its orientation in the image. The filter calculates the mean (μ) and standard deviation (σ) of the nine pixel values in a 3 pixel by 3 pixel window centred on each pixel in the smoothed image to create a new derived image of σ/μ values. Small values of σ/μ correspond to areas which are relatively homogeneous. Larger values indicate areas with greater inhomogeneity that could be related to boundaries around features of interest, for instance the edge of a bright iceberg surrounded by darker sea ice. A threshold value of σ/μ is selected as the criterion to decide which pixels in the image have a neighbourhood with greater inhomogeneity and therefore belong to edges. The outcome of this stage in the edge-detection process is sensitive to the threshold value: too high and boundaries around features will not be detected, or adjacent icebergs will not be separated; too low and the image will be over-segmented, dividing many single features into multiple subsections. The system provides an initial value for this criterion which can then be adjusted by the operator to suit conditions in the sub-region of an image under analysis.

The next stage bonds the individual pixels that satisfy the inhomogeneity criterion into connected edge regions. These regions may be several pixels thick. They are then eroded to leave a precisely defined line one pixel thick, representing the line of maximum local inhomogeneity. This stage of the process produces "edges" which enclose regions, plus a number of edges with free ends. The image is cleaned up to remove these false edges. The final stage groups all pixels within each closed region into a segment of the image and assigns a unique identifier to the segment. Each pixel within the segment is given the same identifier to signify its membership of that segment. Figure 1 shows the results of the segmentation technique applied to a small test region within a SAR image depicting icebergs off the Antarctic coast.

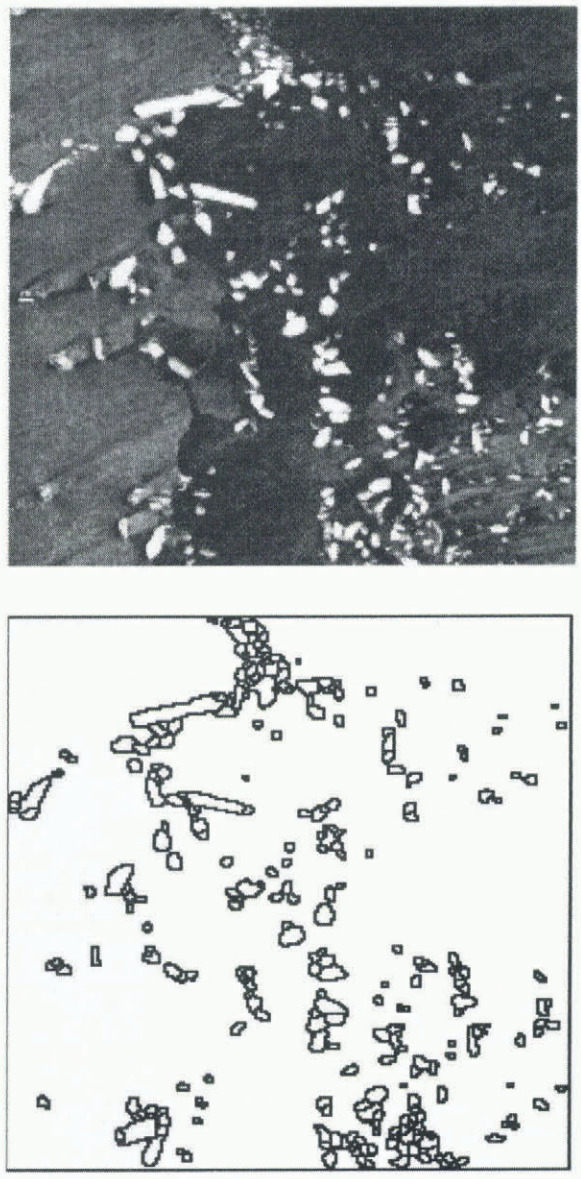

Fig. 1. (a) Part of a SAR image depicting icebergs off the Antarctic coastline southwest of West Ice Shelf, East Antarctica. (b) Outlines of the segments after the application of the segmentation technique to the region in (a). (ERS SAR data © ESA, 1993.)

4. IDENTIFICATION OF ICEBERGS

The segmentation process is applied to the SAR images in a non-discriminatory fashion. That is to say, it identifies closed regions within an image on the basis of the σ/μ value and independently of other properties. These closed regions may represent icebergs, sea ice or open water, or even a mixture of two or more surface types, depending on the homogeneity of the different types of surface and the detection threshold set in the edge-building process. Additional information, such as pixel intensity, is required in order to distinguish icebergs from other segments. A simple threshold test successfully distinguishes segments containing well-defined icebergs with a higher average intensity from the back-

https://doi.org/10.3189/1998AoG27-1-68-74 Published online by Cambridge University Press

ground of lower intensity. A manual verification stage then assesses the remaining segments not accepted by this test. Segments for which icebergs were difficult to identify, or whose outlines were poorly defined because they contained a mix of surface types, were rejected together with those that clearly contained sea ice or open water. Where an individual iceberg had been over-segmented, the separate segments were joined into one iceberg.

Williams and others (personal communication, 1997) found that the basic system described above successfully identified segments containing virtually all the icebergs with a size of 6 pixels (i.e. 0.06 km^2 in area) and more, and many of the icebergs with a size of 4 or 5 pixels. Most of the icebergs with a size of less than 4 pixels were not successfully identified by the segmentation process. The operator can manually identify these missed bergs for re-analysis at a later time. Their statistics are not included in the dataset used in this work. This outcome is consistent with the properties of the sigma-on-mu filter and size of window used in the calculation of σ/μ.

Williams and others (personal communication, 1997) also found that the area of positively identified icebergs was overestimated by about 20% in this segmentation process. In the ideal case, the icebergs would be clearly defined within a background of homogeneous texture so that the segment boundaries would closely match the edges of the icebergs. In reality, the texture can be far from homogeneous so that lines of maximum inhomogeneity need not coincide exactly with the iceberg boundaries. Most of these extraneous pixels can be eliminated on the basis of their intensity properties. In addition, some pixels around the margins of an iceberg will contain a sub-pixel mix of iceberg and background and have an intermediate intensity value. For an accurate estimate of the iceberg size, a portion of these pixels will need to be assigned to the iceberg. It is intended to implement these additional steps in a later refinement of the iceberg-detection system. For this current work the results of the image-analysis system are taken as is.

Thus the qualifications and bias estimates on the numbers and sizes of icebergs identified following the segmentation and verification procedures are:

(a) the minimum iceberg size reliably detected and measured is about 0.06 km^2,

(b) the number of icebergs in the population is underestimated, mostly in the small size classes,

(c) the area of icebergs is overestimated by about 20% on average,

(d) the total area of icebergs identified represents 85–95% of the image population.

5. ICEBERG SPATIAL DISTRIBUTION, NUMBER DENSITY AND AREA DENSITY

The area of each iceberg segment is calculated from the number of pixels in the segment and the size of a pixel, i.e. 100 m by 100 m. The location of an iceberg is given by the position of its centroid. The overall spatial distribution or dispersion of the identified icebergs is presented in terms of their number density in Figure 2 for a cell of size 20 km by 20 km. The number density is the number of icebergs in a cell averaged over all radar scenes that include that cell, or equivalently, the total number of icebergs observed in that

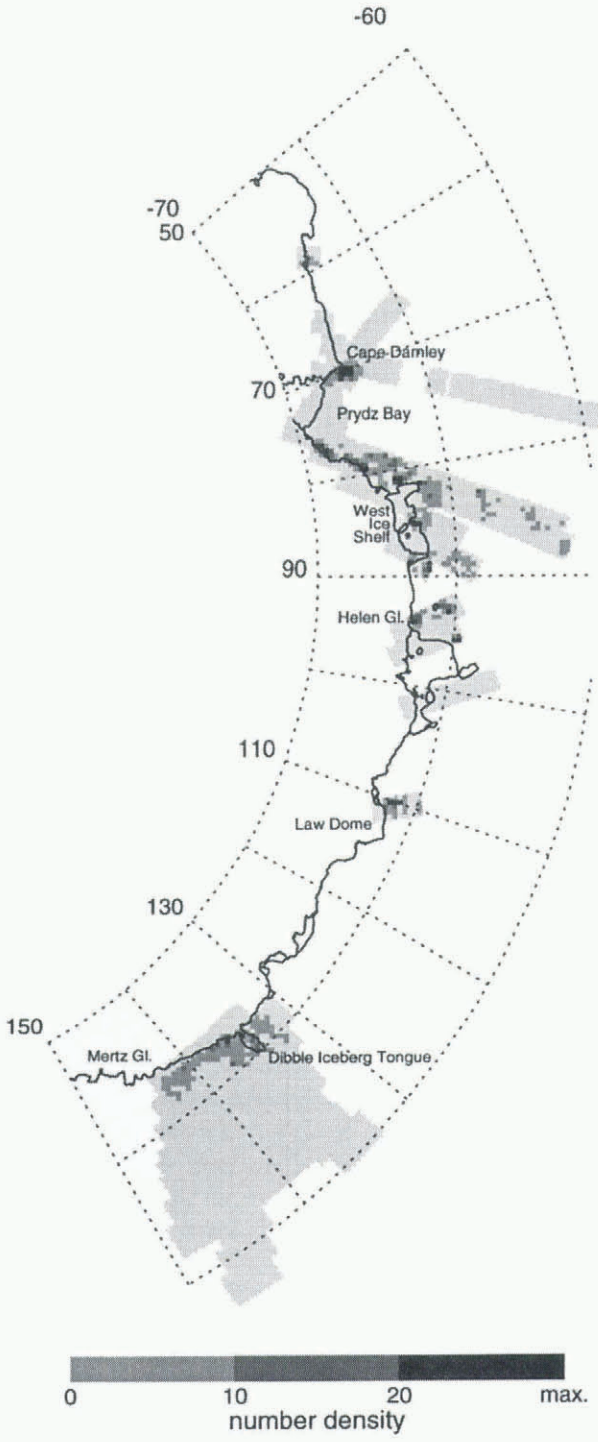

Fig. 2. East Antarctic coastline showing the coverage of the SAR images. The lightest shading indicates that no icebergs were identified in that area. The number density of icebergs identified in the images is shown in the darker shades; it is the number of icebergs observed in each 20 km by 20 km cell averaged over all images containing that cell.

cell from all scenes divided by the number of scenes. This allows for multiple observations of the same iceberg, for instance those that are grounded, and provides a statistical estimate of the likelihood of finding an iceberg in any given cell. The area density is the average area of icebergs in a cell and is calculated by the same process, with each observation weighted by the area of the iceberg segment.

Figure 2 shows that icebergs occur in higher concentrations close to the Antarctic coastline than in regions further north, despite the sparse image coverage. This is most noticeable in the Mertz Glacier sector (130–145° E) where

https://doi.org/10.3189/1998AoG27-1-68-74 Published online by Cambridge University Press

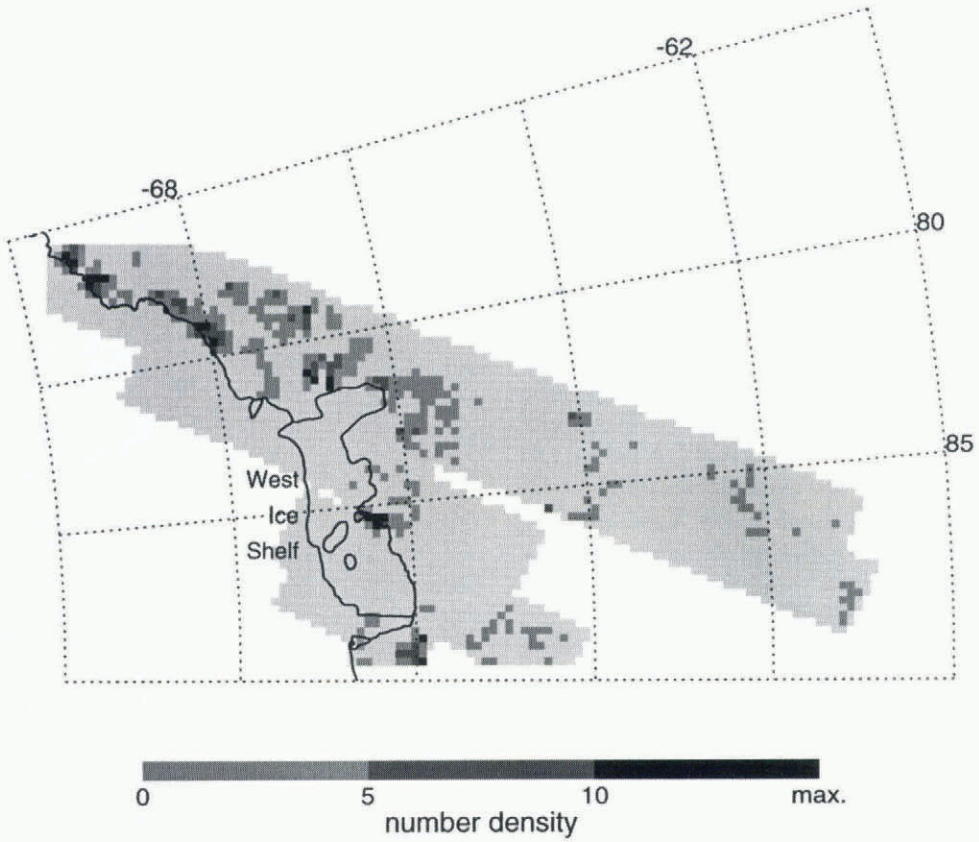

Fig. 3. Number density of icebergs in West Ice Shelf–eastern Prydz Bay sector, showing the clusters of icebergs and the intervening areas with no identified icebergs (lightest shade). The cell size is 10 km by 10 km.

there are virtually no icebergs further than 160 km from the coast. Similarly, off Cape Darnley (70° E) there are virtually no icebergs of detectable size north of 140 km from the coast. By contrast, icebergs occur well north of West Ice Shelf to 61° S, about 550 km off the coast. These broad characteristics of the distribution are consistent with the spatial distribution found from shipboard observations of iceberg occurrences presented by Tolstikov (1966) and updated by Eskin in Koshlyakov (1994), and with the analysis of a large number of observations collected on Australian expedition voyages (Hamley and Budd, 1986).

Figure 3 shows the iceberg density in one of the study regions near West Ice Shelf and Prydz Bay between 75° and 90° E. The concentration of icebergs is high close to the coast and West Ice Shelf, and much lower in the area to the north. The sources of many of the icebergs identified in this area are expected to be the central and eastern parts of West Ice Shelf. The majority of them are carried to the west with the westward continental slope current (Tchernia and Jeannin, 1984; Young and Hyland, 1997), also known as the Antarctic East Wind Drift. The groups of icebergs at 64° and 62° S suggest a preferred drift path carrying them generally northwards to join the Antarctic Circumpolar Current. This pattern contrasts with the virtual absence of icebergs in these latitudes in the next swath of SAR images to the west, approximately at 75° E (Fig. 2). A retroflection in the current has been observed between 85° and 100° E by following the long-term drift of individual icebergs with satellite transponders (Tchernia and Jeannin, 1984) and using observations with the ERS-1 wind scatterometer (Young and Hyland, 1997). The transport of icebergs northwards in this region would explain the tendency of contours of iceberg concentration derived from shipboard observations to be further from the coast between 80° and 105° E.

The icebergs tend to occur in clusters in many of the images. It is likely that the clusters seen in Figure 3, which are located in very deep water north of 66° S, have been generated either by the calving of a number of icebergs from a section of the ice shelf over a short time interval or by the break-up of a larger iceberg into many smaller fragments. The areas of ocean between the clusters are virtually devoid of icebergs of detectable size. Clustering of icebergs also occurs in the region near Mertz Glacier, partly associated with grounding in shallow water. Higher concentrations of icebergs occur in the Dibble Iceberg Tongue (134–135° E) and in the region to the east, upstream of this barrier.

6. ICEBERG SIZE STATISTICS

The area statistics of icebergs identified in images from a single pass of the satellite across the western extremity of West Ice Shelf (about 80° E) are presented as histograms in Figure 4. The area classes are given on a logarithmic scale (base 2) such that each two classes represent a doubling in area. The number of icebergs in each size class is given in Figure 4a. The partitioning of the total area of icebergs between the different size classes is given in Figure 4b.

Figure 4b exhibits a bimodal distribution in the sum of the iceberg areas in each size class. Just two icebergs of area 32–64 km^2 account for 25% of the total area, and a few more icebergs, each greater than 2 km^2, increase that to 40%. This bimodal form reflects the origin of these icebergs and the way they fracture after calving from West Ice Shelf.

https://doi.org/10.3189/1998AoG27-1-68-74 Published online by Cambridge University Press

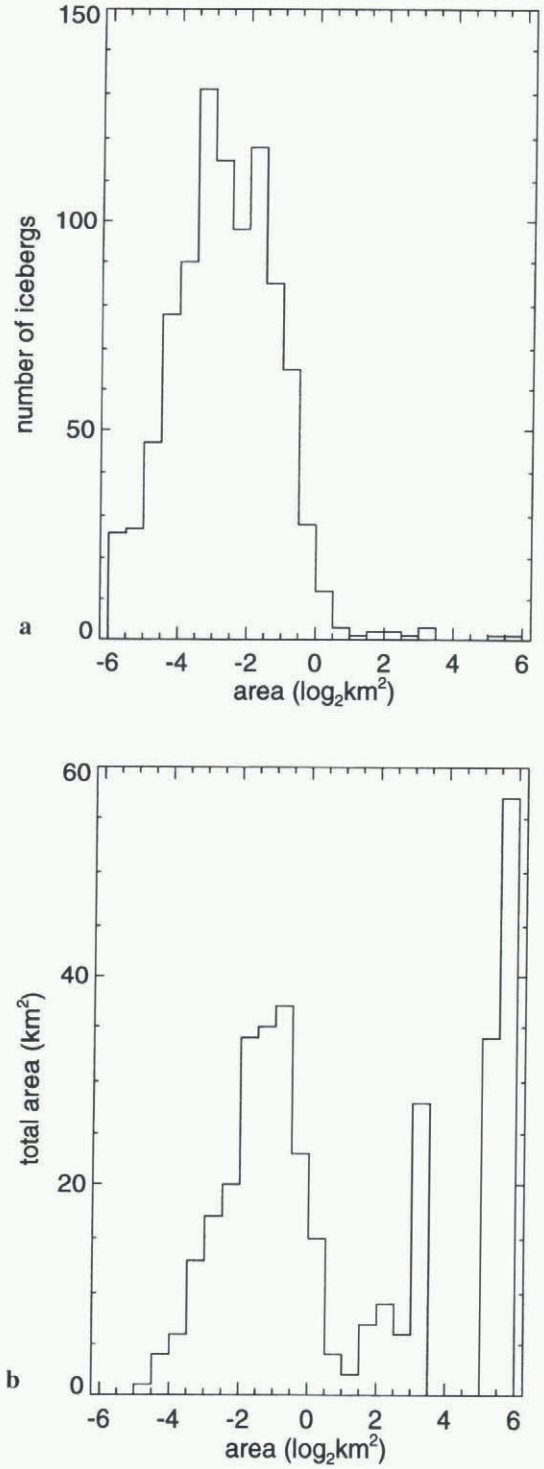

Fig. 4. Size distribution of icebergs identified in images acquired on one orbit of the ERS-1 satellite crossing the western extremity of West Ice Shelf. Area is given on a logarithmic scale (base 2) such that each two increments represent a doubling in area. (a) Number of icebergs in each size category. (b) Integrated area of all icebergs in each size category, showing multimodal character of mass distribution in different size categories.

Large parts of the ice shelf are heavily crevassed. When icebergs calve they sometimes break off in very large sections, or as many small icebergs. One very large iceberg, of area 3500 km^2, retained its identity while grounded for 2 years after calving in May 1994 from the east end of West Ice Shelf. When it began drifting in 1996, a series of advanced very high-resolution radiometer images showed it break into five large fragments and many other icebergs too small to be detected in the images. In this way, icebergs tend to be injected into two discrete size populations to give the bimodal distribution in this region.

Table 1 summarises the area statistics for a number of regions around the coast. High standard-deviation values for some areas indicate the presence of one or more very large icebergs in the sample. Using the median value as an indicator of typical iceberg sizes, the region near Mertz Glacier has significantly larger icebergs than other coastal areas, almost twice as large as those near Law Dome and Cape Darnley. The clusters north of West Ice Shelf (64° and 62° S) also have a higher proportion of large icebergs than areas closer to the coast at the same longitude. The region labelled "Union" represents a large sample of icebergs identified in a set of non-overlapping SAR images selected to avoid any bias from multiple observations of the same icebergs, and to provide a once-only coverage of all the separate regions. The values for this region provide an estimate of iceberg areas in the total population. The statistics do not include a number of mega-icebergs that are known to be present in this sector of East Antarctica, each of which has an area in excess of 1000 km^2.

Table 1. Area statistics of icebergs identified in separate regions of East Antarctica

Region	*Long.* °E	*N*	*Total* km^2	*Median* km^2	*Mean* km^2	*σ* km^2
Cape Darnley	70	705	122.42	0.12	0.17	0.03
West Ice Shelf (coastal)	85	1378	548.50	0.14	0.40	5.64
West Ice Shelf (northwards)	85	73	45.39	0.20	0.62	6.24
Helen Glacier	92	478	124.38	0.18	0.26	0.07
Law Dome	110	334	61.85	0.12	0.19	0.07
Mertz Glacier	140	539	393.30	0.21	0.73	75.50
Union	50–145	3320	1313.09	0.14	0.40	27.91

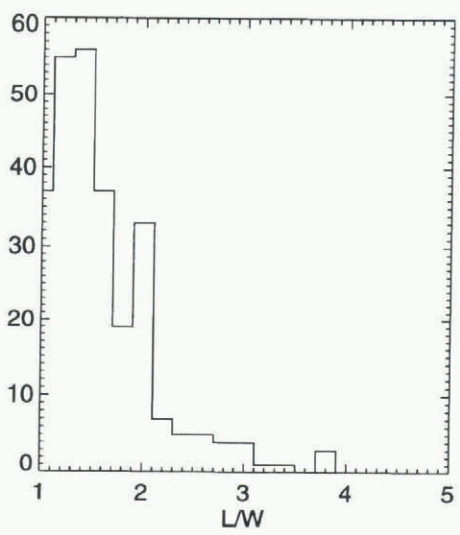

Fig. 5. Length-to-width ratio for icebergs in size class 0.5–1 km^2 for the "Union" dataset.

https://doi.org/10.3189/1998AoG27-1-68-74 Published online by Cambridge University Press

In addition, an estimate of the length and width of the icebergs is obtained from the maximum overall length and the sum of the two orthogonal half-widths. A half-width is defined as the maximum width of the section of iceberg to one side of the length axis orthogonal to that axis. The ratios of length to width (L/W) for the size class 0.5–1 km^2, are presented in Figure 5 for the "Union" set of icebergs. Measurement errors on the length and width of an iceberg are estimated to be ±1.0 pixel. The first and second moments, mean and standard deviation respectively, of the distribution of L/W values are presented in Table 2 for each of four size classes. Given the measurement errors in L and W and therefore L/W, we also calculate the standard errors of the two moments as presented in parentheses in Table 2. The small values of the standard errors indicate that the distributions for different size classes have different mean values, which suggests that there may be some dependence of L/W on size. Also presented in Table 2 is the ratio of mean length to mean width. Using airborne photographic surveys, Dmitrash (1972) found a value for this ratio of 1.60 from a sample of 535 icebergs with mean area of 0.12 km^2 between 39° and 56° E in Enderby Land. He reported a range of values of 1.5–1.6 when results of other authors for samples of smaller numbers of icebergs from different areas were included. The value for size class 0.25–0.5 km^2 (Table 2) is similar to the values reported by Dmitrash, but with the larger size classes included, there is a greater range of values than he reports. The value for all size classes of the "Union" dataset, including sizes smaller than 0.25 km^2, is 1.53.

Table 2. Mean and standard deviation of the distribution of length-to-width ratio for size classes of icebergs in the "Union" dataset, and ratio of mean length to mean width. Standard errors of the calculated mean and standard deviation of each distribution are given in parentheses

Size class km^2	*N*	*Mean L/W*	*Std dev. L/W*	*Mean L/Mean W*
0.25–0.5	620	1.35 (±0.01)	0.29 (±0.01)	1.48
0.5–1.0	269	1.41 (±0.01)	0.34 (±0.02)	1.60
1.0–2.0	71	1.47 (±0.02)	0.40 (±0.03)	1.76
>2.0	24	1.32 (±0.01)	0.33 (±0.01)	1.68

7. CONCLUSION

Analysis of images acquired with SAR during the austral winter has provided new data on the sizes and spatial distribution of icebergs around a large sector of the coast of East Antarctica. The system can reliably detect and measure icebergs with a minimum size of 0.06 km^2, although it underestimates the number of smaller icebergs. There is a significant variation, by up to a factor of two, in the area of icebergs derived from different sections of the ice-sheet margin. The average value of the length-to-width ratio for icebergs in the whole population is similar to previously reported values and shows some variability with size. The probability of finding icebergs is highest close to the coast, in general decreasing with distance from the coast such that few icebergs were detected more than 160 km from the coast. This is consistent with shipboard observations. One sector about 85° E contained icebergs to at least 550 km from the coast, as a result of the transport of icebergs northwards in this region by a retroflection in the westward-heading near-coastal current (East Wind Drift) which connects with the southern margins of the eastward-heading Antarctic Circumpolar Current (West Wind Drift).

ACKNOWLEDGEMENTS

The ERS.SAR.PRI images were supplied by the European Space Agency (ESA) through the ERS Announcement of Opportunity projects ERS.AO.AUS5-1, ERS.AO2.AUS103 and ERS.AO2.AUS105. The SAR data are copyright to ESA, 1993, 1994, 1995.

REFERENCES

Dimitrash, Zh. A. 1972. O gorizontal'nykh razmerakh antarkticheskikh aysbergov po dannym aerofotos" yemki [Horizontal dimensions of Antarctic icebergs according to aerial photosurvey data]. *Inf. Byull. Sov. Antarkt. Eksped.*, **86**, 40–41.

Ferrigno, J. G., B. K. Lucchitta, K. F. Mullins, A. L. Allison, R. J. Allen and W. G. Gould. 1993. Velocity measurements and changes in position of Thwaites Glacier/iceberg tongue from aerial photography, Landsat images and NOAA AVHRR data. *Ann. Glaciol.*, **17**, 239–244.

Hamley, T. C. and W. F. Budd. 1986. Antarctic iceberg distribution and dissolution. *J. Glaciol.*, **32**(111), 242–251.

Hult, J. L. and N. C. Ostrander. 1974. Applicability of ERTS to Antarctic iceberg resources. *In* Freden, S.C. and M.A. Becker, *eds. Third Earth Resources Technology Satellite-1 Symposium. Vol. 1B.* Greenbelt, MD, Goddard Space Flight Center, 1467–1490. (NASA Special Publication SP-351.)

Koshlaykov, M. N., I. M. Belkin, V. M. Radikevich and Yu. A. Romanov. 1994. Icebergs along 67° S in the Pacific sector of the Antarctic in February–March of 1992. *Oceanology*, **33**(6), 720–726.

Lytle, V. I., R. Massom, A. P. Worby and I. Allison. 1997. Floe sizes in the East Antarctic sea ice zone estimated using combined SAR and field data. *In Third ERS Scientific Symposium, 17–21 March 1997, Florence, Italy. Proceedings.* Frascati, Italy, European Space Agency, 931–936. (ESA Publication SP-414.)

Mead, C. 1992. Iceberg distribution analysis using satellite imagery. (Major project dissertation, Royal Melbourne Institute of Technology.)

Orheim, O. 1988. Antarctic icebergs — production, distribution and disintegration. (Abstract.) *Ann. Glaciol.*, **11**, 205.

Phillips, H. A. and S.W. Laxon. 1995. Tracking of Antarctic tabular icebergs using passive microwave radiometry. *Int. J. Remote Sensing*, **16**(2), 399–405.

Rott, H., P. Skvarca and T. Nagler. 1996. Rapid collapse of northern Larsen Ice Shelf, Antarctica. *Science*, **271**(5250), 788–792.

Sephton, A. J., L. M.J. Brown, J. T. Macklin, K. C. Partington, N. J. Veck and W. G. Rees. 1994. Segmentation of synthetic-aperture radar imagery of sea ice. *Int. J. Remote Sensing*, **15**(4), 803–825.

Swithinbank, C., P. McClain and P. Little. 1977. Drift tracks of Antarctic icebergs. *Polar Rec.*, **18**(116), 495–501.

Tchernia, P. and P. F. Jeannin. 1984. Circulation in Antarctic waters as revealed by iceberg tracks, 1972–1983. *Polar Rec.*, **22**(138), 263–269.

Tolstikov, Ye. I., *ed.* 1966. *Atlas Antarktiki I [Atlas of Antarctica I].* Leningrad, Gidrometeorologicheskoye Izdatel'stvo.

Willis, C. J., J. T. Macklin, K. C. Partington, P. G. Teleki, W. G. Rees and R. G. Williams. 1996. Iceberg detection using ERS-1 synthetic aperture radar. *Int. J. Remote Sensing*, **17**(9), 1777–1795.

Young, N. W. and G. Hyland. 1997. Applications of time series of microwave backscatter over the Antarctic region. *In Third ERS Scientific Symposium, 17–21 March 1997, Florence, Italy. Proceedings.* Frascati, Italy, European Space Agency, 1007–1014. (ESA Publication SP-414.)